Clinical Radiology 74 (2019) 409.e7–409.e16

Contents lists available at ScienceDirect

Clinical Radiology

journal homepage: www.clinicalradiologyonline.net

Diagnosis of solitary pulmonary lesions with intravoxel incoherent motion diffusion-weighted MRI and semi-quantitative dynamic contrast-enhanced MRI

S.C. Zhou, Y.J. Wang, T. Ai, L. Huang, T.T. Zhu, W.Z. Zhu, L.M. Xia*

Department of Radiology, Tongji Hospital, Tongji Medical College, Huazhong University of Science and Technology, 1095# Jiefang Road, Qiaokou District, Wuhan, Hubei, China

ARTICLE INFORMATION

Article history:
Received 5 July 2018
Accepted 6 December 2018

AIM: To evaluate the diagnostic value of intravoxel incoherent motion (IVIM) diffusion-weighted (DWI) magnetic resonance imaging (MRI) and semi-quantitative dynamic contrast-enhanced MRI (DCE-MRI) to help diagnose indeterminate solitary pulmonary lesions (SPLs) and the subgroups of lung cancer (LC), and to explore the relationship between IVIM and DCE-MRI.

MATERIALS AND METHODS: Sixty-four consecutive patients (44 male, 20 female; age, 52.77±10.46 years) from February 2014 to September 2016 with SPLs, were involved in this prospective study. Total apparent diffusion coefficient (ADCtotal), tissue diffusivity (D), pseudo-diffusion coefficient (D*), perfusion fraction (F), maximum enhancement ratio (MER), Tmax, slope, and washout were compared between the lung cancer (LC) and benign group and among the subtypes of LC. Time–intensity curves (TICs) were drawn. Receiver operating characteristic (ROC) curves were constructed to estimate the diagnostic performance. The correlation of both tools was assessed.

RESULTS: ADCtotal, D, and Tmax were significantly higher for benignity than for LC (p=0.005, p=0.002 and p<0.001 respectively). D* and slope were significantly higher in LC than benignity (p=0.005 and p=0.011, respectively). D and Tmax had the highest sensitivity and accuracy, respectively. A combination of D and Tmax improved the sensitivity to 90.5%, the specificity to 86.4%, and the accuracy to 89.1%. Poor correlations were found between parameters derived from IVIM and DCE-MRI. ADCtotal values of SCC and SCLC were found to be significantly lower compared with that in adenocarcinoma.

CONCLUSION: Both IVIM-DWI and DCE-MRI were useful for discriminating benignity from LC. ADCtotal was helpful for distinguishing adenocarcinoma and non-adenocarcinoma. A combination of DCE-MRI and IVIM could provide a robust method to determine the microstructural characteristics of SPLs.

* Guarantor and correspondent: L. M. Xia, Tel.: +86 13607176908.
E-mail address: xialiming2018@outlook.com (L.M. Xia).

https://doi.org/10.1016/j.crad.2018.12.022
0009-9260/

Introduction

Lung cancer (LC) is the leading cause of cancer mortality worldwide.[1] CT is the most routine method to assess pulmonary lesions and ^{18}F-fluorodeoxyglucose PET/CT is often used for further definition[2]; however, there are still some solitary pulmonary lesions (SPLs) that show atypical characteristics, including inflammatory or infectious lesions such as active tuberculosis, granuloma, and inflammatory myofibroblastic tumours.[3] Moreover, both methods involve increased radiation burden. Therefore, a further evaluation is needed to reflect the inner microstructure of SPLs non-invasively.

Nowadays, diffusion-weighted imaging (DWI) is used to diagnose tumours in various organs.[4–6] Moreover, it is also a robust tool for the characterisation of LCs, which is comparable with or even better than positron-emission tomography (PET).[7,8] Several studies have demonstrated that DWI is helpful in the differential diagnosis of SPLs.[9,10]

One of the extended models of DWI, the intravoxel incoherent motion (IVIM) technique, has been explored in the evaluation of tumours and shows some promise over conventional apparent diffusion coefficient (ADC).[11,12] IVIM can separately stratify molecular diffusion and microcirculation in the capillary using segmental bi-exponential fitting with multiple b-values.[13] So IVIM is supposed to be more accurate and provide more information of lesion characteristics.

Semi-quantitative dynamic contrast-enhanced MRI (DCE-MRI) using a generalised kinetic model was a study method used to depict perfusion; so far, a few studies have demonstrated its good diagnostic efficiency in lung lesions.[14–16] It is very important to diagnose indeterminate SPL before appropriate management is given. Thus IVIM and semi-quantitative DCE-MRI may provide an improvement in diagnosing indeterminate SPLs, and there may be a relationship between the two methods, especially referring to the perfusion component.

Therefore, the purpose of this study was to explore the diagnostic value of IVIM-DWI and DCE-MRI in differentiating indeterminate SPLs and subsets of LC. In addition, the role of the two methods in diagnosis and their relationship is also discussed.

Materials and Methods

Patients

This prospective study was approved by the Medical Ethics Committee, and written informed consent was obtained from each patient. Between February 2014 and September 2016, 76 consecutive patients detected by multisection computed tomography (MSCT) with indeterminate SPLs were enrolled. The case inclusion criteria were: (a) patients had not received treatment; (b) the short axis diameter was >1 cm on MSCT; (c) patients had no contraindications to MRI; (d) histopathological confirmation was obtained within 7 days after the MRI examination. Indeterminate SPLs were defined by two senior radiologists in consensus (each with >20 years' pulmonary nodules diagnostic experience) on MSCT.

Among them, four patients were excluded because of unsatisfactory imaging quality due to motion artefacts, eight patients were excluded because of lack of histopathological confirmation. The final cases comprised 64 patients (44 male, 20 female; mean age, 52.8±10.5 years). Ten patients (15.6%) received histopathological confirmation by fibrebronchoscope biopsy, two (3.1%) cases were diagnosed by endobroncheal ultrasonography biopsy, three (4.7%) were diagnosed by CT-guided percutaneous transthoracic lung biopsy, 47 (73.4%) underwent surgical lobectomy, and two (3.1%) underwent wedge resection.

MRI

MRI examinations of all patients were performed on a 1.5 T MRI system (GE Healthcare HDx MR, Waukesha, WI, USA) with an eight-channel cardiovascular phased-array coil. The conventional MRI sequences included: transverse electrocardiogram (ECG)-triggered spin echo (SE) T1-weighted imaging (WI), transverse respiratory-triggered fat-suppressed FR fast spin echo (FSE) T2WI, and coronary breath-hold single-shot (SS)FSE T2WI.

IVIM images were acquired by multi-b-factor DWI scans (b=0, 20, 50, 100, 150, 200, 400, 600, 1,000 s/mm^2) using a SS echo-planar imaging pulse sequence (SSEPI) with respiratory trigger and fat suppression. Diffusion sensitive gradients were applied in three orthogonal directions (x,y,z).

DCE MRI was obtained with a fat-suppressed breath-hold axial T1W volume interpolated gradient echo liver acquisition with volume acceleration (LAVA) sequence. After one acquisition as the preference mask, an intravenous bolus injection of gadobenate dimeglumine (0.1 mmol/kg; MultiHance, Bracco SpA, Milano, Italy) was administered at a rate of 2.5 ml/s followed by a 15 ml saline flush using a power injector. DCE MRI images were thereafter obtained 5 seconds after the injection of contrast agent and 15 dynamic phases at an interval of 10 seconds were obtained for each patient. Protocol details are listed in Table 1.

MRI data post-processing

Two radiologists (A and B, with 7 years and 10 years of MRI experience, respectively) who were blinded to the histopathological results performed data analysis by means of consensus. A region of interest (ROI) was drawn manually by author B (S.Z.) on the solid portion of the lesion by referring to DW-IVIM and DCE-MRI on the central section with longest diameter, avoiding visually identified vessels, liquefaction, and necrosis. The drawn ROIs were transferred to all the DW-IVIM and DCE-MRI maps.

IVIM parameters

The ADCtotal value was calculated according to equation (1):

Table 1
MRI protocol parameters.

Sequence	Plane	TR/TE (ms)	Matrix	Thickness/gap (mm)	FOV (mm)	AT (min)
PG-T1WI/SE	Axial	264/8	320×160	5/1	400×400	6
RT-T2WI/FRFSE	Axial	4,500/110	320×224	5/1	400×400	3.6
T2WI/SSFSE	Coronal	2,500/95	380×254	5/1	400× 400	0.35
RT-IVIM	Axial	2,500/76	256×128	5/1	400×400	8.93
3D-LAVA	Axial	4.2/2	256×128	3/0	350×350	6.33

PG, pulse gating; SE, spin echo; RT, respiratory-triggered; FRFSE, fast recovery fast spin echo; SSFSE, single shot fast spin echo; IVIM, intravoxel incoherent motion; 3D-LAVA, three-dimensional liver acquisition with volume acceleration; TR/TE, repetition time/echo time; FOV, field of view; AT, acquisition time.

$$\frac{S(b)}{S0} = e^{-b\times ADCtotal} \quad (1)$$

Where S(b) and S0 represent DWI SI (signal intensity) at a given b-value and b = 0 s/mm^2, respectively.

For the IVIM parameters, the relationship between DWI SI and the b-values were described in equation (2):

$$\frac{S(b)}{S0} = Fe^{-b(D+D*)} + (1-F)e^{-bD} \quad (2)$$

where F is the perfusion fraction, D is the true diffusion coefficient, and D* is pseudo-diffusion coefficient.

All original IVIM data were transferred to a GE Advantage workstation 4.5 and post-processed with MADC software, based on the Levenberg–Marquardt algorithm by a voxel-wise fitting. Segmental bi-exponential models were used to calculate the corresponding ADCtotal, D, D*, and F pseudo-colour pictures based on the quantitative values of each parameter.

DCE-MRI kinetic parameters

DCE-MRI data were post-processed by Markov random fields (MRF) 3D non-rigid registration algorithms supported by GE Healthcare to minimise motion artefact. Then the mean SI of the lesions of each dynamic phase was measured on the operator console by the ROI copied from IVIM to the 15 designated dynamic phases.

The contrast enhancement ratio (ER) was calculated as per equation (3):

$$SI\%(t) = \frac{SI(t) - SI0}{SI0} \times 100\% \quad (3)$$

where SI% (t) is the increased SI percentage over baseline at time t, SI(t) is the SI at time t, and SI0 is the baseline SI measured before contrast injection. Time–intensity curves (TICs) were obtained according to the SI% (t) at each time point. SImax was determined as the maximum SI during the 15 phases and Tmax were defined as the time point of SImax. Other parameters were calculated as follows.[16]

The enhancement ratio at Tmax (maximum enhancement ratio, MER) was calculated as the increased percentage of SI between the SImax and SIo, see equation (4)

$$MER = \frac{SImax - SI0}{SI0} \times 100\% \quad (4)$$

The slope of the TICs was calculated as the increased percentage of SI at the Tmax over the baseline value per second, see equation (5)

$$Slope = \frac{MER}{Tmax} \quad (5)$$

The washout ratio was calculated as the decreased percentage of SI between the SImax and the SI of the end time point, see equation (6)

$$washout = \frac{SImax - SIend}{SImax} \times 100\% \quad (6)$$

When the Tmax was at the end time point, the washout value was set to zero.

DCE-MRI morphology parameters

The enhancement patterns were classified into four types[15]: homogeneous, with the SI of the lesions increasing uniformly; heterogeneous, representing irregular contrast medium distribution with regions of no or low enhancement; peripheral, including thin rim enhancement and grid-like enhancement, representing linear enhancement in the periphery or inside a lesion; and no enhancement, representing no contrast medium uptake in the nodule.

Four patterns were distinguishable from the characteristic of TICs on the basis of the results of phase analysis of the peak enhancement and washout of contrast medium[15,17,18]: type A, a sharp SI increase followed by an obvious washout (slope>1.5 SI%/s and washout ≥10%); type B, an intensive obtuse SI increase with plateau or slightly increase afterward (washout <10%); type C, continuous and incremental SI increase throughout the phrases; and type D, no significant SI increase over baseline (MER<10%; see Fig 1).

Statistical analysis

Statistical analyses were performed by SPSS 19.0 for Windows (SPSS, Chicago, IL, USA) and MedCalc version 15.2 (MedCalc Software, Mariakierke, Belgium). All continuous numeric data were expressed as mean ± standard deviation. The normality and homoscedasticity of data were tested using the Kolmogorov–Smirnov test and Levene's tests, respectively. Student's *t*-test was used in F and MER between benign and malignant groups. The

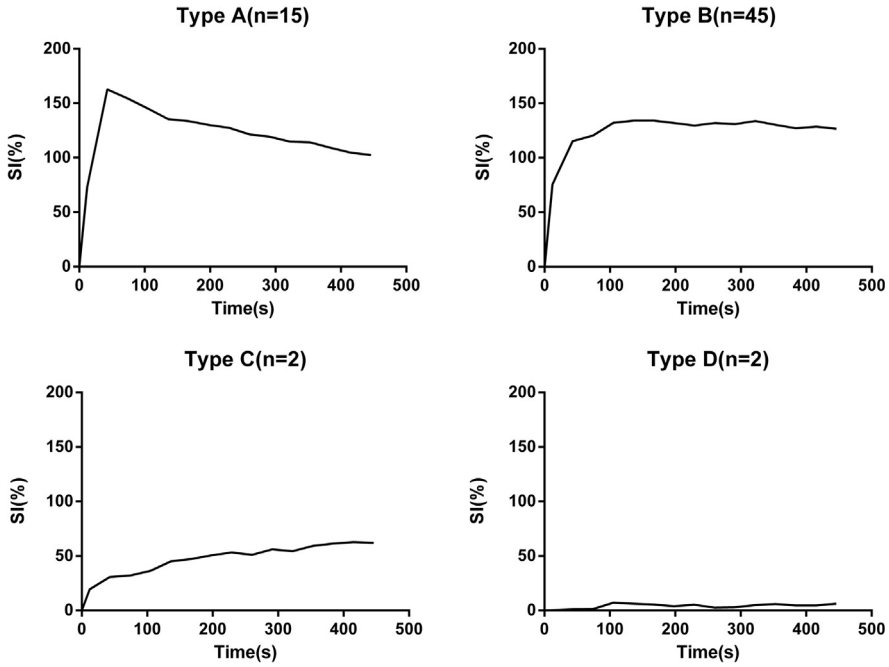

Figure 1 Time–intensity curves for all cases grouped according to curve types A–D.

Mann–Whitney *U*-test was used to evaluate other parameters. TICs were drawn by GraphPad prism Version 6 (GraphPad Software, La Jolla, CA, USA). A generalised Fisher exact test was used to analyse the differences of TIC types and enhancement patterns between malignant and benignity. A *p*-value of <0.05 was considered to indicate a significant difference.

Receiver operating characteristic (ROC) analysis was performed to assess the diagnostic efficacy of IVIM and DCE parameters in differentiating benignity and LCs, and qualified by the areas under the ROC curves (AUC). The optimal cut-off points were determined based on the Youden index. The Pearson correlation test was applied to explore the correlation between the IVIM and DCE parameters. A correlation coefficient *r* of 0–0.5 was considered to indicate a poor correlation, 0.5–0.8 was moderate correlation, and $r>0.8$ was defined as high correlation.

Results

Histopathological findings

Among the 64 SPLs, the final histopathological diagnosis included 42 cases of malignant tumours and 22 benign lesions. The primary malignancies were as follows: squamous cell carcinoma (SCC, $n=11$); adenocarcinoma ($n=16$); small cell carcinoma (SCLC, $n=7$); sarcomatoid carcinoma ($n=3$); large cell carcinoma ($n=1$); typical carcinoid ($n=1$); undifferentiated type non-small cell lung cancer ($n=3$). The benign lesion group included one hamartoma, four sclerosing haemangiomas, one aspergillosis, eight cases of tuberculosis caseation, three lung abscesses, and five inflammatory granulomas.

Morphological findings

A significant difference ($p=0.022$) was found between malignancy and benignity. A peripheral enhancement pattern was found in the cases of non-adenocarcinoma (grid-like pattern) and in caseous necrosis of tuberculosis (thin rim pattern). Eight of 11 cases of SCC (72.7%), five of seven cases of NSCLC (71.4%), and three cases of sarcomatoid carcinoma showed grid-like enhancement. Three of the seven cases of tuberculosis manifested thin rim enhancement. Fifteen of the 16 cases of adenocarcinoma showed the heterogeneous pattern (see Fig 2).

Type A ($n=15$) curves were only seen in malignancy, type B ($n=45$) were seen in both malignancy and benignity, type C ($n=2$) and type D ($n=2$) curves were only seen in benignity. A significant difference of curve type (A–D) was found between malignant and benign lesions ($p<0.001$; Figs 2 and 3; Table 2).

Quantitative parameters

ADCtotal and D values were significantly lower in LCs than in benignity (ADCtotal: 1.30 ± 0.40 versus $1.64\pm0.57\times10^{-3}$ mm^2/s, $p=0.007$; D: 0.88 ± 0.29 versus $1.19\pm0.43\times10^{-3}$ mm^2/s, $p=0.003$). D* values were higher in LCs compared with that in benignity (50.7 ± 46.1 versus $26.2\pm30\times10^{-3}$ mm^2/s, $p=0.019$); however, no significant differences were found in F values between the two groups (34.1 ± 16.4 versus 43.0 ± 27.2%, $p=0.106$).

The Tmax values obtained from LCs were significantly shorter than those of benignity (131.6 ± 83.4 versus 273 ± 110 seconds, $p<0.001$), the slope values were significantly higher in malignancy than those in benignity (1.38 ± 1.06 versus 0.8 ± 0.72%/s, $p=0.021$). No significant differences

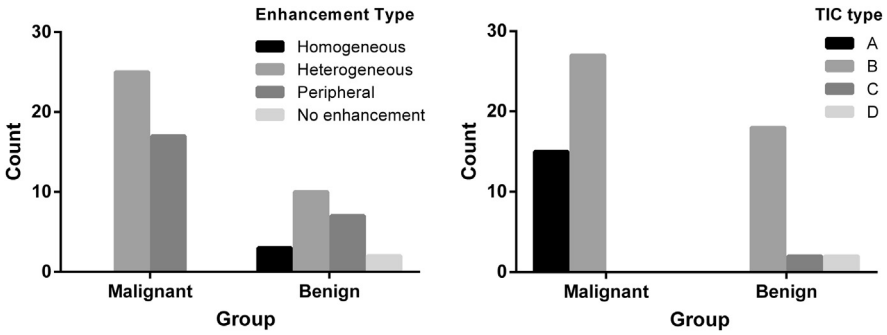

Figure 2 Histogram of enhancement and TICs types distribution in malignant and benign lesions group. The left graph shows heterogeneous and peripheral enhancement can be found in both LC and benignity; however, grid-like enhancement of peripheral type can only be found in LC and thin rim enhancement can only be seen in benignity. Besides, homogeneous and no enhancement are only seen in benignity. The right graph shows only type A can be seen in LC, type C and D can only be seen in benignity, there is an overlap of type B TICs in LC and benignity.

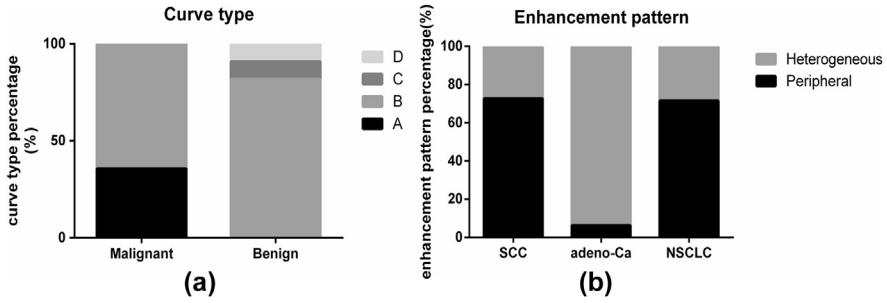

Figure 3 Percentage stacked graph of curve types and enhancement patterns in different groups of SPLs. (a) Percent stacked graph of different types of TICs distributed in malignant and benign pulmonary lesions showed that type A curves were only seen in malignancy, type B curves were see in both malignancy and benignity, type C and D curves only appeared in benignity and were rarely seen. (b) Percent stacked graph of different enhancement pattern manifested in SCC, adenocarcinoma and NSCLC subgroup of lung cancer, demonstrating adenocarcinoma mainly showed heterogeneous enhancement, SCC and NSCLC were mainly manifested as peripheral pattern.

Table 2
Frequency of TICs pattern according to diagnosis.

Diagnosis	Type A	Type B	Type C	Type D
Malignant	15	27		
SCC	4	7		
Adenocarcinoma	5	11		
SCLC	3	4		
Sarcoma-Ca		3		
Carcinoid	1			
Large cell carcinoma		1		
NSCLC (undefined)	2	1		
Benign		18	2	2
Sequestration		1		
Hamartoma		1		
Sclerosing haemangioma		4		
inflammatory granuloma		5		
Focal haemorrhage				1
Abscess		3	1	
Tuberculosis		4	1	1

SCC, squamous cell carcinoma; adenocarcinoma, adenocarcinoma; SCLC, small cell lung cancer; Sarcoma-Ca, sarcomatoid carcinoma; NSCLC, non-small cell lung cancer.

Table 3
Measurements of IVIM-DWI and DCE-MRI parameters in malignant SPLs and benign groups.

Variable	Malignant (n=42)	Benign (n=22)	p-Value
IVIM-DWI			
ADCtotal (10^{-3} mm^2/s)	1.30±0.40	1.64±0.57	0.007[a]
D (10^{-3} mm^2/s)	0.88±0.29	1.19±0.43	0.003[a]
D* (10^{-3} mm^2/s)	50.7±46.1	26.2±30.0	0.019[a]
F (%)	34.1±16.4	43.0±27.2	0.106
DCE-MRI			
MER (%)	121.4±49.8	149.5±116.5	0.232
Tmax (s)	131.6±83.4	273.0±110.0	0.000[a]
Slope (%/s)	1.38±1.06	0.80±0.72	0.021[a]
Washout (%)	7.31±6.23	5.51±4.17	0.392

IVIM-DWI, intravoxel incoherent motion diffusion weighted imaging; DCE-MRI, dynamic contrast-enhanced MR imaging; ADCtotal, apparent diffusion coefficient calculated by multi-b value in the protocol; D, true diffusion coefficient; D*, pseudo-diffusion coefficient; F, perfusion fraction; MER, maximum enhancement ratio.

[a] Statistically significant at p=0.05.

were found in MER and washout between the two groups (MER: 121.4±49.8 versus 149.5±116.5%, p=0.232; washout: 7.31±6.23 versus 5.51±4.17%, p=0.392). The IVIM values and DCE parameters for both groups are shown in Table 3 and Fig 4 and a representative case is shown in Fig 5.

To identify different pathological subtypes of lung cancer, all IVIM- and DCE-related parameters among squamous cell carcinoma (SCC), adenocarcinoma (adenocarcinoma), and small cell lung cancer (SCLC) were compared. ADCtotal values of SCC and SCLC were found to be significant lower compared with that in adenocarcinoma (SCC: 1.23±0.41×10^{-3} mm^2/s,

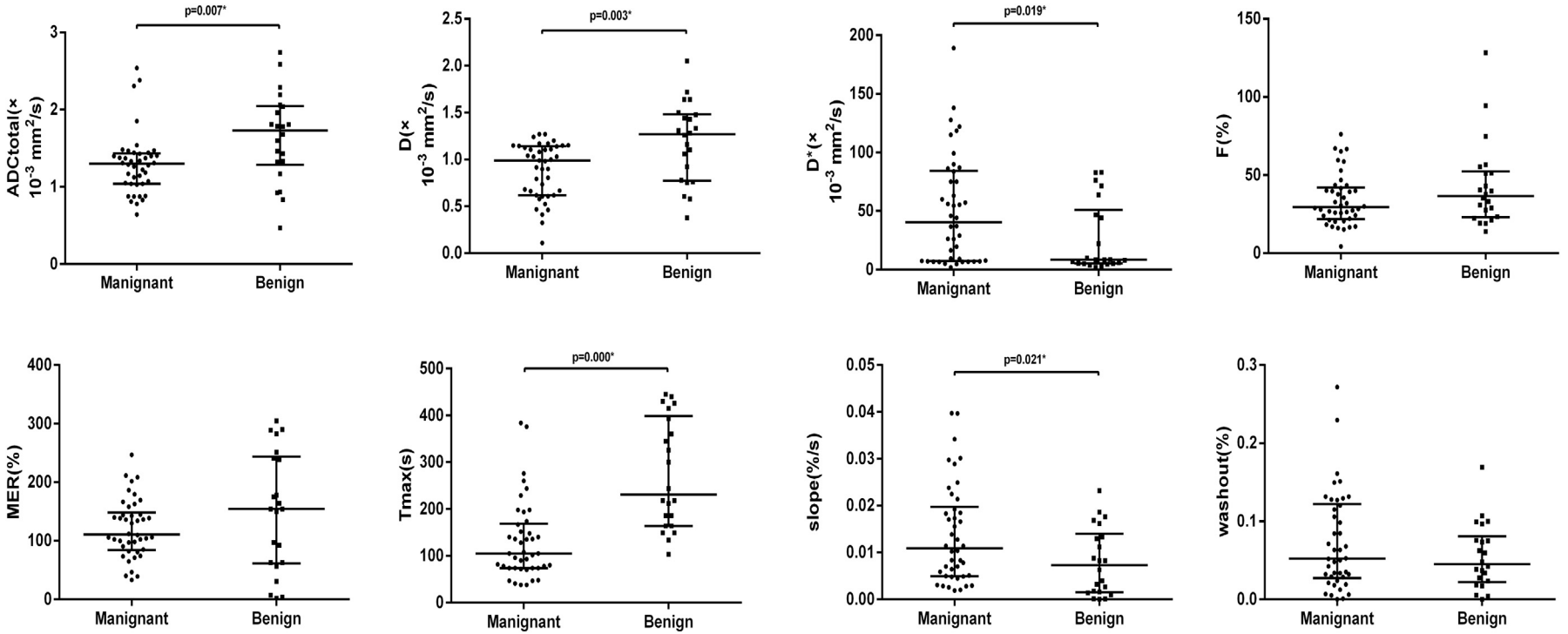

Figure 4 Scatter plots of ADCtotal, D, D*, F, MER, Tmax, slope and washout values in LC and benign lesions. Top and bottom lines are 25 and 75 percentiles of the data, respectively. Line in the middle represents median value. LC showed lower ADCtotal, D, shorter Tmax, higher D* and slope ($p \leq 0.05$). Other parameters showed no significant difference.

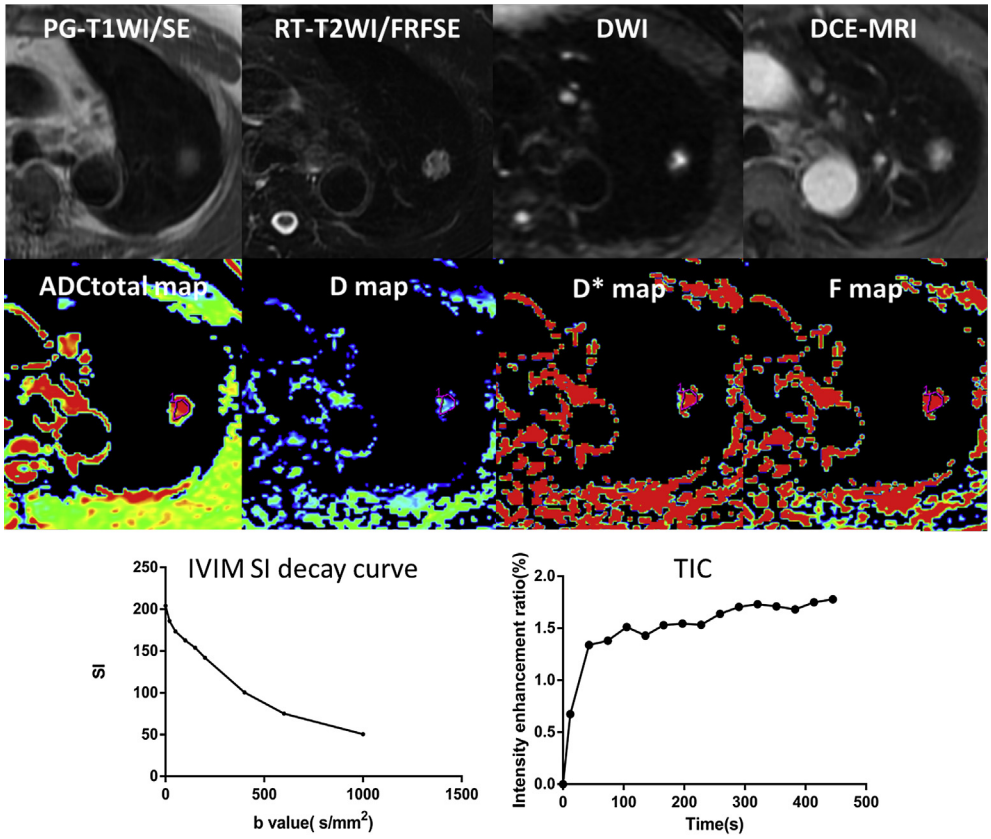

Figure 5 PG-T1WI/SE image,RT-T2WI/FRFSE image, a DW image (b=500 s/mm^2)of multi-b values, a phase of DCE-MR image, ADCtotal map, D map, D*map, F map, IVIM signal–intensity decay curve and TIC in a 53-year-old man with inflammatory granuloma in left upper lobe of lung. The lesion showed intermediate T1 and mixed slightly higher T2 signal. High DWI signal and heterogeneous enhancement. ROI was placed in the central slice covering the longest diameter of the lesion. The signal intensity decay showed in accordance with IVIM model and the TIC manifested as type B.

SCLC: 1.12±0.4×10^{-3} mm^2/s, adenocarcinoma: 1.47±0.43×10^{-3} mm^2/s, SCC versus adenocarcinoma: p=0.048, SCLC versus adenocarcinoma: p=0.022), no difference was revealed between SCC and SCLC. None of other indices were found to be significantly different between SCC, adenocarcinoma, and SCLC (see Table 4).

Table 4
IVIM-DWI parameters and DCE-MRI parameters in different sub-group of malignant pulmonary lesions.

Variable	SCC	Adenocarcinoma	SCLC	p-Value
ADCtotal (10^{-3} mm^2/s)	1.23±0.41	1.47±0.43	1.12±0.40	0.033[a]
D (10^{-3} mm^2/s)	0.95±0.32	0.99±0.28	0.71±0.28	0.061
D* (10^{-3} mm^2/s)	54.4±36.4	52; 9±52.4	40.3±29.1	0.764
F (%)	31.2±20.4	34.5±18.0	34.2±13.9	0.713
MER (%)	114.4±60.3	117.4±55.4	121.7±35.8	0.869
Tmax (s)	127.3±53.8	145.6±114.5	128.7±80.9	0.922
Slope (%/s)	1.20±0.98	1.39±1.10	1.45±1.24	0.870
Washout (%)	7.23±5.09	6.38±7.36	8.39±4.68	0.297

IVIM-DWI, intravoxel incoherent motion diffusion weighted imaging; DCE-MRI, dynamic contrast-enhanced MR imaging; ADCtotal, apparent diffusion coefficient calculated by multi-b value in the protocol; D, true diffusion coefficient; D*, pseudo-diffusion coefficient; F, perfusion fraction; MER, maximum enhancement ratio; adenocarcinoma, adenocarcinoma; SCLC, small cell lung cancer.
[a] Statistically significant at p=0.05.

As Type B TICs showed great overlap between the two groups, further analysis on the "indeterminate, Type B" lesions using IVIM and DCE parameters was undertaken. D, MER, and Tmax values of LC were significantly lower than those of benignity (D: 0.89±0.29 versus 1.23±0.38×10^{-3} mm^2/s, p=0.001; MER: 103.2±42.9% versus 168.9±96.9%, p=0.013; Tmax: 159.6±90.3 versus 252±110.5 seconds, p=0.004), and D* values of LC were significantly higher than those of benignity (55.3±42.6 versus 26.9±29.8×10^{-3} mm^2/s, p=0.014; Table 5).

Diagnostic performances of MRI parameters and correlation between IVIM and DCE-MRI parameters

The ROC analysis of IVIM and DCE-MR parameters for distinguishing malignancy from benignity expanded the diagnostic performances of multi indices. AUC of ROC analysis of IVIM and DCE parameters ranged from 0.676 to 0.854. D had the highest sensitivity (95.2%) and Tmax had the best accuracy (63.6%). The results are summarised in Table 6 and Fig 6. The combination of D and Tmax improved the AUC to 0.921, the sensitivity to 90.5%, the specificity to 86.4%, and the accuracy to 89.1%.

According to the results of TICs types, taking the type A TICs as LC, type C and D TICs as benignity, the diagnostic

Table 5
Comparison of IVIM-DWI and DCE-MRI Parameters between malignant SPLs and benign groups showing Type-B curves.

Variable	Malignant (n=27)	Benign (n=18)	p-Value
IVIM-DWI			
ADCtotal (10^{-3} mm^2/s)	1.28±0.33	1.56±0.57	0.069
D (10^{-3} mm^2/s)	0.89±0.29	1.23±0.38	0.001[a]
D* (10^{-3} mm^2/s)	55.3±42.6	26.9±29.8	0.014[a]
F (%)	34.0±16.7	39.4±28.6	0.835
DCE-MRI			
MER (%)	103.2±42.9	168.9±96.9	0.013[a]
Tmax (s)	159.6±90.3	252.0±110.5	0.004[a]
Slope (%/s)	0.93±0.80	0.93±0.72	1.000
Washout (%)	4.13±2.96	5.07±3.11	0.314

IVIM-DWI, intravoxel incoherent motion diffusion weighted imaging; DCE-MRI, dynamic contrast-enhanced MR imaging; ADCtotal, apparent diffusion coefficient calculated by multi-b value in the protocol; D, true diffusion coefficient; D*, pseudo-diffusion coefficient; F, perfusion fraction; MER, maximum enhancement ratio.
[a] Statistically significant at p=0.05.

Table 6
Diagnostic performance of multiparameters for differentiation of malignancy from benignity.

Variable	AUC	Cut-off value	Sensitivity	Specificity	Accuracy
ADCtotal (10^{-3} mm^2/s)	0.708	1.57	90.5%	59.1%	79.7%
D (10^{-3} mm^2/s)	0.729	1.25	95.2%	54.5%	81.3%
D* (10^{-3} mm^2/s)	0.680	8.82	71.4%	59.1%	67.2%
Tmax (s)	0.854	205	85.7%	63.6%	78.1%
Slope (%/s)	0.676	0.42	83.3%	45,5%	70.3%
D+Tmax	0.921		90.5%	86.4%	89.1%

ADCtotal, apparent diffusion coefficient calculated by multi-b value in the protocol; D, true diffusion coefficient; D*, pseudo-diffusion coefficient; AUC, area under receiver operating characteristic.

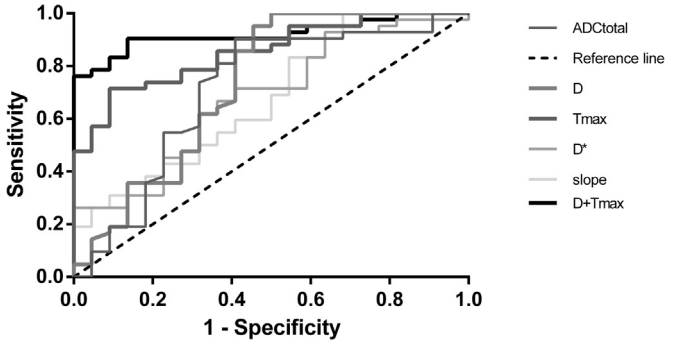

Figure 6 Receiver operating characteristic (ROC) curves of IVIM and DCE parameters for discriminating benign from malignant pulmonary lesions. Tmax had the largest AUC, D had the highest sensitivity and accuracy, and Tmax had the highest specificity. The combination of D and Tmax provided the best sensitivity, specificity, and accuracy.

performance of all the parameters to differentiate overlapped type B curve indeterminate SPNs were further analysed using ROC analysis. The combination of D and MER provided the highest sensitivity (92.6%) and accuracy (84.4%). The combination of D and Tmax provide highest specificity (77.8%; see Table 7).

The correlation test showed that the ADCtotal was found to have poor correlation with the MER (r=0.272, p=0.03), no significant correlation was observed among other indices between the two methods. The correlation coefficient r ranged from −0.137 to 0.216 and the p-value ranged from 0.055 to 0.985.

Table 7
Diagnostic performance of multiparameters for differentiation of type B indeterminate SPNs.

Variable	AUC	Cut-off value	Sensitivity	Specificity	Accuracy
D (10^{-3} mm^2/s)	0.771	1.16	85.2%	61.1%	75.6%
D* (10^{-3} mm^2/s)	0.718	8.82	81.5%	55.6%	71.1%
MER (%)	0.704	145.0	92.6%	66.7%	82.2%
Tmax (s)	0.750	208.0	77.8%	55.6%	68.9%
D+MER	0.819	0.526	92.6%	72.2%	84.4%
D+Tmax	0.872	0.564	85.2%	77.8%	82.2%

D, true diffusion coefficient; D*, pseudo-diffusion coefficient; MER, maximum enhancement ratio; D+MER, combination of D and MER; D+Tmax, combination of D and Tmax.

Discussion

The present study found that multiparametric DW-IVIM and DCE-MRI in differentiation of indeterminate SPLs is feasible. Morphologically, TICs and enhancement type were significantly different between LCs and benignity. Quantitatively, LCs had predominant decreases in ADCtotal, D, and Tmax combining with increases in D* and slope when compared with benignity. Adenocarcinoma had lower ADCtotal values than those of SCC and SCLC. A combination of IVIM and DCE-MRI can significantly improve the diagnostic efficacy of SPLs. Poor correlation was found between IVIM and DCE derived metrics.

Semi-quantitative DCE-MRI provided better diagnostic performance of the single parameter derived from DCE-MRI (AUC of ROC analysis: 0.676–0.854, sensitivity 83.3–85.7%, accuracy 70.3–78.1%) compared with quantitative DCE-MRI according to a similar previous study,[19] and combination of IVIM and DCE-MRI parameters in differential diagnosis give the comparable efficacy (AUC 0.921, sensitivity 90.5%, specificity 86.4%, and accuracy 89.1%). This demonstrated that the easiest and most accessible semi-quantitative DCE-MRI can provide comparable performance to quantitative DCE-MRI, without the complex scanning setting and post-processing procedure. Moreover, the TICs were more intuitive than numerical parameters, which can be easily hand drawn, indicating that semi-quantitative DCE-MRI can replace quantitative DCE-MRI in differentiating clinical lung lesions. Few studies have been published to date on this subject and it needs to be proven in future studies.

In addition to the above results, morphologically, four types of TICs were obtained. Type A curves indicated lung cancer, with the washout value threshold at 0.1 SI%/s, revealed a specificity of 100% because no benignity reached this level, no active infection showed washout in the present study. Both type C and D curves suggested a benign diagnosis, including hamartoma, sclerosing haemangioma, inflammatory granuloma, abscess, and tuberculosis, with a specificity of 100%. Meanwhile, enhancement pattern was also helpful for differential diagnosis, especially in

diagnosing tuberculosis (thin-rim pattern indicate a caseation, a central necrosis with a peripheral annular zone consisted with granuloma, fibres, and inflammatory substance) and subtypes of lung cancer (grid-like pattern prompt a non-adenocarcinoma diagnosis, indicating central tumour nests or aggregative growth tumour cells and peripheral fibrous septa or compressive atelectasis), although it was not specific. In addition, based on the TICs, kinetic parameters can be derived for estimates of tissue perfusion and permeability. A previous study[16] reported that the first half of the TIC (i.e., MER, Tmax, and slope value) correlated with tumour angiogenesis, and that of the latter half (i.e., washout value) correlated with the tumour interstitium. The number of microvessels was found to be correlated with the MER and the slope value of the TIC, and this number correlated negatively with the Tmax. A shorter Tmax and a larger slope was found in LCs compared with benignity, reflecting hypervascularity and increased permeability in LCs, Ohno *et al.*[14] analysed MER and slope in lung cancer and benignity containing active infection. They reported that active infection showed complete overlap with the malignant SPNs when MER and slope were evaluated, as both had increased blood flow, perfusion, and capillary permeability at radiopathological, pharmacokinetic, and pathological studies. In present study, only four cases of active infection were included so the slope was still found to be significantly different between two groups. Furthermore, the real process of pulmonary lesions is complex because of the dual blood circulation in the lung. Thus, more cases of various types of benignity could be collected to assessing perfusion differences among various groups.

A strong negative correlation between tumour cellularity and the ADC value was found in previous studies.[20] Thus decreased ADCtotal and D values in LC can be interpreted as increased cellularity and decreased extracellular space in LC compared with benign lesions. Among different subgroups of lung cancer, adenocarcinoma had higher ADCtotal values than SCC and SCLC, similar to a previous meta-analysis.[10] The result may due to lower cellularity of adenocarcinoma than those of SCC and SCLC, which was consistent with previous studies.[21,22] In IVIM theory, D* was considered to be proportional to the blood velocity and capillary segment length.[13] The increased D* in LC may result from angiogenesis of immature vessels in LC, accordingly the blood flow velocity and capillary segment length was larger in LC. In addition, D* is sensitive to movement, therefore, MRI during free breathing may also increase D* noise and make it inaccurate. Using respiratory trigger during IVIM in the present study may produce more reliable D* and result in different results compared with previous study.[19,23] F is the perfusion fraction referring to the vascular volume fraction. F did not reflect significant features in differentiating lung cancer from benignity, which is consistent with previous studies,[19,23,24] but F showed a higher value in benign lesions, consistent with a previous study.[25] One reason may be due to hypervascular benignity, such as inflammatory granuloma and sclerosing haemangiomas, contributing to a large portion of the benign populations. Lesions with a rich blood supply are usually characterised by abundant vascular structures, including increased blood flow, increased capillary permeability, and vasodilation. Another possible reason may be that the F value is affected by relaxation effects and the T2 contribution.

D* and F derived from IVIM and DCE parameters are all parameters related to perfusion, so some connections were deduced between the two kinds of metrics; however, poor correlation was observed between the perfusion-related indices. Several previous studies[19,24] have reported similar results. The reasons may be because of (1) poor reproducibility of D* and F measurements[26]; (2) the parameters are based on different mechanisms, D* was proportional to the blood velocity and capillary segment length, F referred to the vascular volume ratio, while DCE parameters are based on the quantity, distribution, and permeability of microvessels, elastic fibres, and collagen fibres within the tumour; (3) D* and F comprise other physiological process, such as D* includes the blood supply components of the parenchyma and F is more exactly the ratio of the volume of MRI-visible water flowing in each voxel.[23]

This study has some limitations. First, the ROIs were drawn in the central slice and the mean value was used, which might lead to bias owing to tumour heterogeneity, and did not contain the entire volume. Second, the number of cases was limited, and there was an imbalance between the LC (42) and benign group (22). Therefore, a larger-scale study is necessary to confirm these findings. Furthermore, the same protocol should be applied using different vendors to measure the stability of diagnostic performance.

In conclusion, IVIM and semi-quantitative DCE-MRI were helpful in the determination of indeterminate SPLs. ADCtotal could be useful for distinguishing adenocarcinoma and non-adenocarcinoma. A combination of IVIM and DCE-MRI can provide a differential diagnosis for indeterminate SPLs.

Conflict of interest

The authors declare no conflict of interest.

Acknowledgements

The present study was supported by the by National Basic Research Program of China (2015CB931802) and by grants from the National Natural Scientific Foundation of China (No. 81401388 and No.81471637).

References

1. Siegel RL, Miller KD, Jemal A. Cancer statistics. *CA Cancer J Clin* 2016;**66**:7–30.
2. Yi CA, Lee KS, Kim BT, *et al*. Tissue characterization of solitary pulmonary nodule: comparative study between helical dynamic CT and integrated PET/CT. *J Nucl Med* 2006;**47**:443–50.
3. Kim HS, Lee KS, Ohno Y, *et al*. PET/CT versus MRI for diagnosis, staging, and follow-up of lung cancer. *J Magn Reson Imaging* 2015;**42**:247–60.
4. Kang SK, Zhang A, Pandharipande PV, *et al*. DWI for renal mass characterization: systematic review and meta-analysis of diagnostic test performance. *AJR Am J Roentgenol* 2015;**205**:317–24.
5. Barentsz MW, Taviani V, Chang JM, *et al*. Assessment of tumor morphology on diffusion-weighted (DWI) breast MRI: diagnostic value of reduced field of view DWI. *J Magn Reson Imaging* 2015;**42**:1656–65.

6. Schelhorn J, Best J, Reinboldt MP, *et al*. Does diffusion-weighted imaging improve therapy response evaluation in patients with hepatocellular carcinoma after radioembolization? Comparison of MRI using Gd-EOB-DTPA with and without DWI. *J Magn Reson Imaging* 2015;**42**:818–27.
7. Mori T, Nomori H, Ikeda K, *et al*. Diffusion-weighted magnetic resonance imaging for diagnosing malignant pulmonary nodules/masses: comparison with positron emission tomography. *J Thorac Oncol* 2008;**3**:358–64.
8. Chen GX, Wang MH, Zheng T, *et al*. Diffusion-weighted magnetic resonance imaging for the detection of metastatic lymph nodes in patients with lung cancer: a meta-analysis. *Mol Clin Oncol* 2017;**6**:344–54.
9. Uto T, Takehara Y, Nakamura Y, *et al*. Higher sensitivity and specificity for diffusion-weighted imaging of malignant lung lesions without apparent diffusion coefficient quantification. *Radiology* 2009;**252**:247–54.
10. Shen G, Jia Z, Deng H. Apparent diffusion coefficient values of diffusion-weighted imaging for distinguishing focal pulmonary lesions and characterizing the subtype of lung cancer: a meta-analysis. *Eur Radiol* 2016;**26**:556–66.
11. Granata V, Fusco R, Catalano O, *et al*. Intravoxel incoherent motion (IVIM) in diffusion-weighted imaging (DWI) for hepatocellular carcinoma: correlation with histologic grade. *Oncotarget* 2016;**7**:79357–64.
12. Broncano J, Luna A, Sanchez-Gonzalez J, *et al*. Functional MR imaging in chest malignancies. *Magn Reson Imaging Clin N Am* 2016;**24**:135–55.
13. Le Bihan D, Breton E, Lallemand D, *et al*. Separation of diffusion and perfusion in intravoxel incoherent motion MR imaging. *Radiology* 1988;**168**:497–505.
14. Ohno Y, Hatabu H, Takenaka D, *et al*. Solitary pulmonary nodules: potential role of dynamic MR imaging in management initial experience. *Radiology* 2002;**224**:503–11.
15. Schaefer JF, Vollmar J, Schick F, *et al*. Solitary pulmonary nodules: dynamic contrast-enhanced MR imaging—perfusion differences in malignant and benign lesions. *Radiology* 2004;**232**:544–53.
16. Fujimoto K, Abe T, Muller NL, *et al*. Small peripheral pulmonary carcinomas evaluated with dynamic MR imaging: correlation with tumor vascularity and prognosis. *Radiology* 2003;**227**:786–93.
17. Donmez FY, Yekeler E, Saeidi V, *et al*. Dynamic contrast enhancement patterns of solitary pulmonary nodules on 3D gradient-recalled echo MRI. *AJR Am J Roentgenol* 2007;**189**:1380–6.
18. Coolen J, Vansteenkiste J, De Keyzer F, *et al*. Characterisation of solitary pulmonary lesions combining visual perfusion and quantitative diffusion MR imaging. *Eur Radiol* 2014;**24**:531–41.
19. Yuan M, Zhang YD, Zhu C, *et al*. Comparison of intravoxel incoherent motion diffusion-weighted MR imaging with dynamic contrast-enhanced MRI for differentiating lung cancer from benign solitary pulmonary lesions. *J Magn Reson Imaging* 2016;**43**:669–79.
20. Yi Y, Sedlaczek O, Muller B, *et al*. Tumor cell load and heterogeneity estimation from diffusion-weighted MRI calibrated with histological data: an example from lung cancer. *IEEE Trans Med Imaging* 2018;**37**:35–46.
21. Matoba M, Tonami H, Kondou T, *et al*. Lung carcinoma: diffusion-weighted mr imaging—preliminary evaluation with apparent diffusion coefficient. *Radiology* 2007;**243**:570–7.
22. Chen LH, Zhang JQ, Chen YF, *et al*. Relationship between apparent diffusion coefficient and tumour cellularity in lung cancer. *PLoS One* 2014;**9**:e99865.
23. Wan Q, Deng YS, Zhou JX, *et al*. Intravoxel incoherent motion diffusion-weighted MR imaging in assessing and characterizing solitary pulmonary lesions. *Sci Rep* 2017;**7**:43257.
24. Wang LL, Lin J, Liu K, *et al*. Intravoxel incoherent motion diffusion-weighted MR imaging in differentiation of lung cancer from obstructive lung consolidation: comparison and correlation with pharmacokinetic analysis from dynamic contrast-enhanced MR imaging. *Eur Radiol* 2014;**24**:1914–22.
25. Deng Y, Li X, Lei Y, *et al*. Use of diffusion-weighted magnetic resonance imaging to distinguish between lung cancer and focal inflammatory lesions: a comparison of intravoxel incoherent motion derived parameters and apparent diffusion coefficient. *Acta Radiol* 2016;**57**:1310.
26. Jiang J, Yin J, Cui L, *et al*. Lung cancer: short-term reproducibility of intravoxel incoherent motion parameters and apparent diffusion coefficient at 3T. *J Magn Reson Imaging* 2018 Apr;**47**(4):1003–12.